Image Deblurring in the Presence of Salt-and-Pepper Noise

Leah Bar[1], Nir Sochen[2], and Nahum Kiryati[1]

[1] School of Electrical Engineering
[2] Dept. of Applied Mathematics
Tel Aviv University, Tel Aviv 69978, Israel

Abstract. The problem of image deblurring in the presence of salt and pepper noise is considered. Standard image deconvolution algorithms, that are designed for Gaussian noise, do not perform well in this case. Median type filtering is a common method for salt and pepper noise removal. Deblurring an image that has been preprocessed by median-type filtering is however difficult, due to the amplification (in the deconvolution stage) of median-induced distortion. A unified variational approach to salt and pepper noise removal and image deblurring is presented. An objective functional that represents the goals of deblurring, noise-robustness and compliance with the piecewise-smooth image model is formulated. A modified L^1 data fidelity term integrates deblurring with robustness to outliers. Elements from the Mumford-Shah functional, that favor piecewise smooth images with simple edge-sets, are used for regularization. Promising experimental results are shown for several blur models.

1 Introduction

Consider an image that has been blurred and contaminated by salt and pepper noise. Typical sources of blur are defocus and motion [3]. Salt and pepper noise is a common model for the effects of bit errors in transmission, malfunctioning pixels and faulty memory locations [5].

Significant attention has been given to image deblurring in the presence of Gaussian noise [3]. We focus on variational methods, that have an important role in modern image deblurring research, see e.g. [20, 21, 23, 14]. Most methods rely on the standard model $g = h * f + n$, that is applicable to a large variety of image degradation processes that are encountered in practice. Here h represents a known space-invariant blur kernel (point spread function), f is an ideal version of the observed image g and n is (usually Gaussian) noise. In this research, we focus on the case of salt and pepper noise.

The assumption of Gaussian noise is a fundamental element of common image deblurring algorithms. It is therefore not surprising that those algorithms produce inadequate results in the presence of salt and pepper noise. This fact is illustrated in Fig. 1. The top-left image in Fig. 1 is the 256×256 *Lena* image, blurred by a pill-box kernel of radius 3 (7×7 kernel) and contaminated

Fig. 1. Current image deblurring algorithms fail in the presence of salt and pepper noise. *Top-left:* Blurred image with Gaussian noise. *Top-right:* Restoration using the method of [23]. *Bottom-left:* Blurred image with salt and pepper noise. *Bottom-right:* Restoration using the method of [23].

by Gaussian noise. Successful restoration is obtained using the state of the art deblurring method of [23] (top-right). The bottom-left image in Fig. 1 is the same blurred Lena image, now contaminated by salt and pepper noise of density 0.01. In this case restoration using the method of [23] is clearly inadequate (bottom-right). Note that due to the inadequacy of the noise model, the algorithm of [23] yields poor results even at lower salt and pepper noise density. The regularization constants used to obtain Fig. 1 (top-right) and (bottom-right) are the same: 10^{-3}. Note that increasing the constant in the presence of salt and pepper noise effectively disables deblurring, while only reducing the amplitude of the noise.

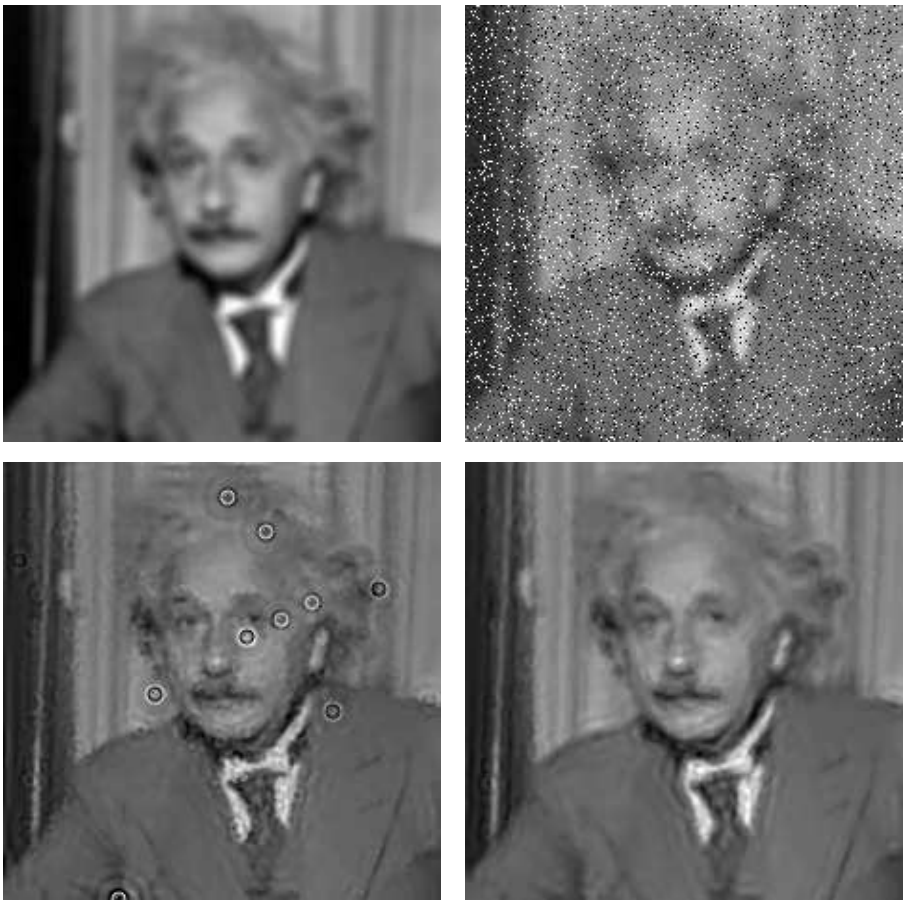

Fig. 2. The failure of the two-stage approach to salt-and-pepper noise removal and image deblurring. *Top-left:* Blurred image. *Top-right:* Blurred image contaminated by salt and pepper noise. *Bottom-left:* The outcome of 3×3 median filtering, followed by deblurring. *Bottom-right:* The outcome of 5×5 median filtering, followed by deblurring.

Salt and pepper noise removal is considered in the literature by itself. It is commonly approached using median-type filters, see e.g [9, 13, 18]. Recently, a promising variational method for impulse denoising was proposed by [7, 16, 17].

In the absence of unified algorithms for deblurring and salt-and-pepper noise removal, the straightforward approach is to first denoise the image, then to deblur it. This two-stage method is however prone to failure, especially at high noise density. Image denoising using median-type filtering creates distortion that depends on the neighborhood size; this error can be strongly amplified by the deblurring process, even in regularized methods. Consider the example shown in Fig. 2. The top-left image is the 256×256 *Einstein* image, blurred using a

pill-box kernel of radius 4. The blurred image with added salt and pepper noise (noise density 0.11) is shown top-right. The outcome of 3×3 median filtering followed by deblurring using the algorithm of [23] is shown bottom-left. At this noise level, the 3×3 neighborhood size of the median filter is insufficient, the noise is not entirely removed, and the residual noise is greatly amplified by the deblurring process. If the neighborhood size of the median filter is increased to 5×5, the noise is fully removed, but the distortion leads to inadequate deblurring (bottom-right).

In this paper we present a unified method for image deblurring and salt-and-pepper noise removal. Using a variational technique, we introduce a cost functional that represents the goals of deblurring, robustness to salt and pepper noise, and compliance with a piecewise-smooth image model. Experimental results exhibit effective image recovery, with various blur models and noise levels.

2 Unified Variational Framework

Image deblurring is an inverse problem, that can be formulated as a functional-minimization problem. Let Ω denote a rectangular domain in $\mathbb{R}^2$, on which the image intensity function $f : \Omega \rightarrow [0, 1]$ is defined. Ideally, the recovered image $\hat{f}$ satisfies

$$\hat{f} = \arg\min_f \int_\Omega \Phi(h * f - g) dA, \tag{1}$$

where $\Phi(\cdot)$ is a metric representing data-fidelity. In the case of Gaussian noise, a quadratic data-fidelity term is used:

$$\Phi(h * f - g) = (h * f - g)^2. \tag{2}$$

The inverse problem represented by Eq. 1 is known to be ill-posed: small perturbations in the data may produce unbounded variations in the solution. To alleviate this difficulty, a regularization term, that reflects some a-priori preferences, is added. The functional to be minimized thus takes the form

$$\mathcal{F} = \int_\Omega \Phi(h * f - g) dA \ + \alpha \mathcal{J}(f) \tag{3}$$

where $\mathcal{J}(f)$ is the regularization operator and α is positive weighting scalar. Several regularization terms were suggested in the literature, for example Tikhonov [22] L^2 smoothness, Total variation (TV) L^1 norm [20, 21], modified L^1 norm [1] and recently an integrated TV and wavelet coefficients regularization [10, 11, 14].

In the presence of salt and pepper noise, the quadratic data-fidelity term (2) is inadequate. In this paper, we use a robust (modified L^1 norm) data-fidelity term

$$\Phi(h * f - g) = \sqrt{(h * f - g)^2 + \eta^2} \ , \tag{4}$$

where η is a small constant. The modified L^1 norm shares the robustness to outliers of the L^1 norm, but avoids the resulting PDE from being singular at

zero. Brox et al [6] have recently used the modified L^1 norm as a fidelity term for precise optical flow estimation.

The regularization terms that we use represent preference for piecewise-smooth images with simple edge sets. In the Mumford-Shah [15] functional, piecewise smooth images are favored by the term $\int_{\Omega \setminus K} |\nabla f|^2 dA$, where K is the edge set. The simplicity of the edge set is maintained in the Mumford-Shah functional by the line integral term $\int_K d\sigma$.

Ambrosio and Tortorelli [2] used the Γ-convergence framework to approximate the irregular Mumford-Shah functional by a sequence of regular functionals. The edge set K is approximated by a smooth auxiliary function v, where $v(x) \approx 0$ if $x \in K$ and $v(x) \approx 1$ otherwise. Mumford-Shah regularization, using the Γ-convergence approximation, has been recently used in electrical impedance tomography [19] and in blind image restoration [4].

The unified functional is

$$\mathcal{F}_\epsilon(f, v) = \int_\Omega \Phi(h * f - g)\, dA \;+\; \beta \int_\Omega v^2 |\nabla f|^2 dA \;\; + \\ +\;\; \alpha \int_\Omega \left(\epsilon |\nabla v|^2 \;+\; \frac{(v-1)^2}{4\epsilon} \right) dA. \tag{5}$$

The first term in the functional is the modified L^1 data-fidelity term (4). The second term favors a piecewise smooth solution and corresponds to the term $\int_{\Omega \setminus K} |\nabla f|^2 dA$ in the Mumford-Shah functional. The third term maintains the simplicity of the edge set and corresponds to the line integral term $\int_K d\sigma$. Here ϵ is a small positive constant, and α and β are positive weights.

3 Minimization techniques

The objective functional (5) depends on the functions f (recovered image) and v (approximated edge map). Minimization with respect to both f and v is carried out using the Euler-Lagrange (E-L) equations (6) and (8), subject to the Neumann boundary conditions $\partial v / \partial N = 0$, $\partial f / \partial N = 0$, where N denotes the normal to the boundary.

$$\frac{\delta \mathcal{F}_\epsilon}{\delta v} = 2\,\beta\, v\, |\nabla f|^2 + \alpha \left(\frac{v-1}{2\epsilon} \right) - 2\,\epsilon\,\alpha\,\nabla^2 v = 0 \tag{6}$$

$$\frac{\delta \mathcal{F}_\epsilon}{\delta f} = \Phi'(h * f - g) * h(-x, -y) - 2\beta\, \mathrm{Div}(v^2\, \nabla f) = 0 \tag{7}$$

Substituting the modified L^1 norm (4) yields

$$\frac{\delta \mathcal{F}_\epsilon}{\delta f} = \frac{(h * f - g)}{\sqrt{(h * f - g)^2 + \eta^2}} * h(-x, -y) - 2\beta\, \mathrm{Div}(v^2\, \nabla f) = 0\ . \tag{8}$$

Studying the objective functional (5), it can be seen that it is convex and lower bounded with respect to either of functions f and v if the other one is

fixed. For example, given v, $\mathcal{F}_\epsilon$ is convex and lower bounded with respect to f. Therefore, following [8], the alternate minimization (AM) approach can be applied: in each step of the iterative procedure we minimize with respect to one function and keep the other one fixed.

Obviously, Eq. (6) is a linear partial differential equation with respect to v. On the contrary, (8) is a nonlinear integro-differential equation. Linearization of this equation is carried out using the fixed point iteration scheme, as in [23, 8]. We set $f = f^l$ in the denominator, and $f = f^{l+1}$ elsewhere, where l is the current iteration number. Eq. (8) can thus be rewritten as

$$\mathcal{H}(v, f^l) f^{l+1} = G(f^l), \quad l = 0, 1, ... \tag{9}$$

where $\mathcal{H}$ is the linear integro-differential operator

$$\mathcal{H}(v, f^l) f^{l+1} = \frac{h * f^{l+1}}{\sqrt{(h * f^l - g)^2 + \eta^2}} * h(-x, -y) - 2\beta \operatorname{Div}(v^2 \nabla f^{l+1})$$

and

$$G(f^l) = \frac{g}{\sqrt{(h * f^l - g)^2 + \eta^2}} * h(-x, -y).$$

Note that (9) is now a *linear* integro-differential equation in f^{l+1}.

The two E-L equations (6) and (8) have now become two linear PDE's, that can be represented by two systems of linear equations. These systems are solved in alternation. This leads to the following iterative algorithm:

`Initialization:` $f^0 = g, \quad v^0 = 1.$

`1. Solve the Helmholtz equation for` v^{n+1}

$$(2\beta |\nabla f^n|^2 + \frac{\alpha}{2\epsilon} - 2\,\alpha\,\epsilon\,\nabla^2)\, v^{n+1} = \frac{\alpha}{2\epsilon}$$

`2. Set` $f^{n+1,0} = f^n$ `and solve for` f^{n+1} `(iterating on` l`)`

$$\mathcal{H}(v^{n+1}, f^{n+1,l}) f^{n+1,l+1} = G(f^{n+1,l}) \tag{10}$$

`3. if` $(||f^{n+1} - f^n||_{L_2} < \varepsilon_1 ||f^n||_{L_2})$ `stop.`

Here ε_1 is a small positive constant. Steps 1 and 2 both call for a solution of a system of linear equations. Step 1 was implemented using the Minimal Residual algorithm [24]. As for step 2, following Vogel and Oman [23], Eq. (10) can be expressed in a quasi-Newton like form

$$f^{n+1,l+1} = f^{n+1,l} - \left[\mathcal{H}(v^{n+1}, f^{n+1,l})\right]^{-1} R(v^{n+1}, f^{n+1,l}) \tag{11}$$

where

$$R(v, f) = \frac{(h * f - g)}{\sqrt{(h * f - g)^2 + \eta^2}} * h(-x, -y) - 2\beta \operatorname{Div}(v^2 \nabla f)$$

and $\mathcal{H}(\cdot,\cdot)$ is the approximation of the Hessian operator. It can be shown that the operator $\mathcal{H}(\cdot,\cdot)$ is self-adjoint and positive definite. Consequently $\mathcal{H}(\cdot,\cdot)^{-1}R(\cdot,\cdot)$ in (11) was computed via the Conjugate Gradients method.

Let f_{ij} denote the discretized image function. The forward and backward finite difference approximations of the derivatives $\partial f(x,y)/\partial x$ and $\partial f(x,y)/\partial y$ are respectively denoted by $\Delta^x_{\pm} f_{ij} = \pm(f_{i\pm1,j} - f_{ij})$ and $\Delta^y_{\pm} f_{ij} = \pm(f_{i,j\pm1} - f_{ij})$. Hence, the discrete form of Eq. (6) is

$$2\beta v_{ij}\left[(\Delta^x_+ f_{ij})^2 + (\Delta^y_+ f_{ij})^2\right] + \alpha \cdot \frac{v_{ij}-1}{2\epsilon} - 2\alpha\epsilon\left(\Delta^x_- \Delta^x_+ v_{ij} + \Delta^y_- \Delta^y_+ v_{ij}\right) = 0,$$

and $\mathrm{Div}(v^2\,\nabla f)$ in Eq. (8) is approximated by

$$\left(\Delta^x_+(v^2_{ij}\Delta^x_-) + \Delta^y_+(v^2_{ij}\Delta^y_-)\right) f_{ij}.$$

In the discrete case, the Neumann boundary conditions were implemented as follows. The observed image was extended by adding margins that are a few pixels wide. These margins were obtained by replicating the one-pixel thick outer frame of the image. The margins were then convolved with the blur kernel. To avoid artifacts, in the presence of salt and pepper noise, care should be taken to ensure that the outer frame of the image is noise free. This limited task can easily be achieved using a median filter.

All convolution procedures were performed in the Fourier Transform domain. The algorithm was implemented in the MATLAB environment.

4 Experimental Results

The performance of the algorithm is presented in Figs. 3, 4 and 5. Fig. 3 (left) is a blurred and noisy version of the *Einstein* image. The blur kernel was a pill-box of radius 4; the noise density was 0.11. Fig. 3 (right) is the outcome of the suggested method. The parameters were $\beta = 0.5, \alpha = 0.5, \epsilon = 0.1$. The superiority of the proposed method, with respect to the sequential one (Fig. 2), is clear.

In all the examples in this section, the convergence tolerance of $\varepsilon_1 = 1 \cdot 10^{-4}$ was reached with 3-5 external iterations (over n). The number of internal iterations (over l) was set to 5. The constant η (Eq. 4) was set to 10^{-4}.

The examples presented in Fig. 4 demonstrate the performance of the algorithm at a variety of noise levels. The images in the left column were all blurred by a pill-box kernel of radius 3. The noise densities were, from top to bottom, 0.01, 0.1 and 0.3. The corresponding recovered images are shown in the right column. Despite the large variability of the noise level, the stability of the algorithm allowed to use the same parameter set in the three cases: $\beta = 0.5, \alpha = 0.5, \epsilon = 0.1$, as in the previous example.

Recovery of motion blur in the presence of salt and pepper noise is demonstrated in Fig. 5. The 256×256 *cameraman* image was blurred by a motion blur kernel of length=8, oriented at an angle $\theta = 25^o$ with respect to the horizon. The blurred image was further contaminated by salt and pepper noise of

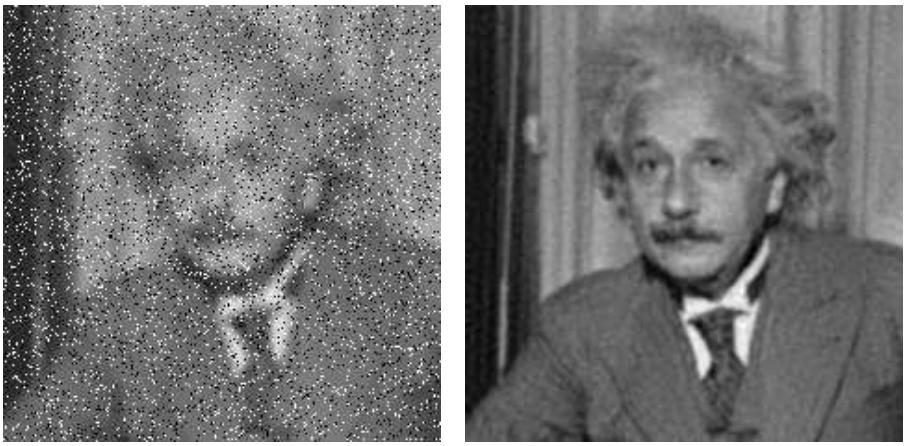

Fig. 3. Deblurring in the presence of salt and pepper noise. *Left:* Source image, blurred with a pill-box kernel of radius 4, and contaminated by noise of density 0.11. *Right:* Recovered image, using the suggested algorithm.

density 0.1 (top-left). The outcome of the method suggested in this paper (with $\beta = 0.6, \alpha = 0.01, \epsilon = 0.1$) is shown top-right. The inadequacy of the sequential strategy, of median filtering followed by conventional deconvolution is demonstrated in the bottom row. The left image in that row is the outcome of 3×3 median filtering followed by the well known Lucy-Richardson restoration (Matlab: `deconvlucy`). The right image in the bottom row was obtained in a similar way, but with a 5×5 median filter.

5 Discussion

We presented a method for image deblurring in the presence of salt and pepper noise. Our unified approach to deblurring and outlier removal is novel and unique. Experimental results demonstrate the superiority of the suggested method with respect to a sequential approach, in which median-based noise removal and image deconvolution are separate steps.

The algorithm is fast, robust and stable. Computation time for 256×256 images is about 3 minutes, using interpreted MATLAB on a 2GHz PC. The robustness of the algorithm is demonstrated by the fact that similar parameters can be used in the processing of different images. For example, the same parameter were used in Fig. 3 and in the three cases shown in Fig. 4. Furthermore, note the fast numerical convergence in our experiments.

In the variational approach, image deblurring in the presence of noise is expressed as a functional minimization problem. The functional consists of a data fidelity term and a regularization term, that stabilizes the inherent ill-posedness of the image deconvolution problem. The data fidelity term used in

Fig. 4. *Left column:* The *Lena* image, blurred with a pill-box kernel of radius 3, and contaminated by salt and pepper noise. The noise densities are (top to bottom) 0.01, 0.1 and 0.3. *Right column:* The corresponding recovered images.

Fig. 5. The case of motion blur. *Top-left:* Blurred and noisy image. *Top-right:* Restoration using the proposed method. *Bottom-left:* The outcome of 3×3 median filtering followed by Lucy-Richardson restoration (Matlab: `deconvlucy`). *Bottom-right:* The outcome of 5×5 median filtering followed by Lucy-Richardson restoration.

this study is the modified L^1 norm. It is more robust than the common L^2 norm for images contaminated by outliers, and yet it is still differentiable and convex.

Elements from the Mumford-Shah segmentation functional, in the Γ-convergence formulation, served as the regularization term. They reflect the profound piecewise-smooth image model. Unlike total variation, the alternative edge-preserving stabilizer, the selected regularization term does not induce nonlinearity beyond that of the fidelity term. An additional advantage of this method is the production of the auxiliary function v, that is an approximated edge map corresponding to the image. For example, Fig. 6 shows the v-maps obtained during the processing of the blurred and noisy *Lena* (pill-box blur,

Fig. 6. Approximated edge maps obtained as a by-product of the restoration process. *Left:* The v-function that corresponds to the deblurring of the *Lena* image with a pill-box kernel and noise density 0.1. *Right:* The v-function that corresponds to the deconvolution of the *Cameraman* image with motion-blur and noise density 0.1.

Fig. 4) and *Cameraman* (motion-blur, Fig. 5) images. Finally, Mumford-Shah regularization has profound theoretical advantages with respect to other edge preserving methods. These aspects will be discussed in the full-length version of this paper.

6 Acknowledgment

This research was supported by MUSCLE: Multimedia Understanding through Semantics, Computation and Learning, a European Network of Excellence funded by the EC 6th Framework IST Programme. It was supported also by the Israel Science Foundation. Leah Bar was supported by the Weinstein Center for Signal Processing Research at Tel Aviv University.

References

1. R. Acar and C.R. Vogel, "Analysis of Total Variation Penalty Methods", *Inverse Problems*, Vol.10, pp. 1217-1229, 1994.
2. L. Ambrosio and V.M. Tortorelli, "Approximation of Functionals Depending on Jumps by Elliptic Functionals via Γ-Convergence", *Communications on Pure and Applied Mathematics*, Vol. XLIII, pp. 999-1036, 1990.
3. M. Banham and A. Katsaggelos, "Digital Image Restoration", *IEEE Signal Processing Mag.*, Vol. 14, pp. 24-41, 1997.
4. L. Bar, N. Sochen and N. Kiryati, "Variational Pairing of Image Segmentation and Blind Restoration", Proc. ECCV'2004, Prague, Czech Republic, Part II: *LNCS* #3022, pp. 166-177, Springer, 2004.

5. G.R. Arce, J.L. Paredes and J. Mullan, "Nonlinear Filtering for Image Analysis and Enhancement", in A.L. Bovik (Ed.), *Handbook of Image & Video Processing*, Academic Press, 2000.
6. T. Brox, A. Bruhn, N. Papenberg and J. Weickert, "High Accuracy Optical Flow Estimation Based on a Theory for Warping", Proc. ECCV'2004, Prague, Czech Republic, Part IV: *LNCS* #3024, pp. 25-36, Springer, 2004.
7. R.H. Chan, C. Ho and M. Nikolova, "Salt-and-Pepper Noise Removal by Median-type Noise Detectors and Detail-preserving Regularization", to appear.
8. T.F. Chan and C. Wong, "Total Variation Blind Deconvolution", *IEEE Trans. Image Processing*, Vol. 7, pp. 370-375, 1998.
9. T. Chen and H.R. Wu, "Space Variant Median Filters for the Restoration of Impulse Noise Corrupted Images", *IEEE Trans. Circuits and Systems II*, Vol. 48, pp. 784-789, 2001.
10. S. Durand and J. Froment, "Reconstruction of Wavelet Coefficients Using Total Variation Minimization", *SIAM Journal of Scientific Computing*, Vol. 24, pp. 1754-1767, 2003.
11. S. Durand and M. Nikolova, "Restoration of Wavelet Coefficients by Minimizing a Specially Designed Objective Function", Proc. IEEE Workshop on Variational, Geometric and Level Set Methods in Computer Vision, pp. 145-152, 2003.
12. F. Malgouyres, "Minimizing the Total Variation Under a General Convex Constraint", *IEEE Trans. Image Processing*, Vol. 11, pp. 1450-1456, 2002.
13. H. Hwang and R. A. Haddad, "Adaptive Median Filters: New Algorithms and Results", *IEEE Trans. Image Processing*, Vol. 4, pp. 499-502, 1995.
14. J. Bect, L. Blanc-Feraud, G. Aubert and A. Chambolle, "A l^1-Unified Variational Framework for Image Restoration", Proc. ECCV'2004, Prague, Czech Republic, Part IV: *LNCS* #3024, pp. 1-13, Springer, 2004.
15. D. Mumford and J. Shah, "Optimal Approximations by Piecewise Smooth Functions and Associated Variational Problems", *Communications on Pure and Applied Mathematics*, Vol. 42, pp. 577-684, 1989.
16. M.Nikolova, "Minimizers of Cost-Functions Involving Nonsmooth Data-Fidelity Terms: Application to the Processing of Outliers", *SIAM Journal on Numerical Analysis*, Vol. 40, pp. 965-994, 2002.
17. M. Nikolova, "A Variational Approach to Remove Outliers and Impulse Noise", *Journal of Mathematical Imaging and Vision*, Vol. 20, pp. 99-120, 2004.
18. G. Pok, J.-C. Liu and A.S. Nair, "Selective Removal of Impulse Noise based on Homogeneity Level Information", *IEEE Trans. Image Processing*, Vol. 12, pp. 85-92, 2003.
19. L. Rondi and F. Santosa, "Enhanced Electrical Impedance Tomography via the Mumford-shah Functional", *ESAIM: Control, Optimization and Calculus of Variations*, Vol. 6, pp. 517-538, 2001.
20. L. Rudin, S. Osher and E. Fatemi, "Non Linear Total Variation Based Noise Removal Algorithms", *Physica D*, Vol. 60, pp. 259-268, 1992.
21. L. Rudin and S. Osher, "Total Variation Based Image Restoration with Free Local Constraints", *Proc. IEEE ICIP*, Vol. 1, pp. 31-35, Austin TX, USA, 1994.
22. A. Tikhonov and V. Arsenin, "Solutions of Ill-posed Problems", New York, 1977.
23. C. Vogel and M. Oman, "Fast, Robust Total Variation-based Reconstruction of Noisy, Blurred Images", *IEEE Trans. Image Processing*, Vol. 7, pp. 813-824, 1998.
24. E.W. Weisstein *et al*, "Minimal Residual Method", from *MathWorld–A Wolfram Web Resource*. `http://mathworld.wolfram.com/MinimalResidualMethod.html`